Materials Today Communications 45 (2025) 112322

Contents lists available at ScienceDirect

Materials Today Communications

journal homepage: www.elsevier.com/locate/mtcomm

# Consolidation behavior of HA-PLA nanocomposites during cold sintering process: Influence of HA-to-PLA ratio and the plasticizing effect of PLA

Muthusundar Kumar [a,b,*], Mohamed Aymen Ben Achour [b], Vedi Ölmez [c], Marie Lasgorceix [b], Rosica Mincheva [a], Anne Leriche [b], Jean-Marie Raquez [a,**]

[a] *Laboratory of Polymeric and Composite Materials, Centre of Innovation and Research in Materials and Polymers, University of Mons, Place du Parc 23, Mons 7000, Belgium*
[b] *Université Polytechnique Hauts-de-France, INSA Hauts-de-France, CERAMATHS-DMP, Valenciennes F-59313, France*
[c] *Belgian Ceramic Research Center, Avenue Gouverneur Cornez 4, Mons 7000, Belgium*

ARTICLE INFO

*Keywords:*
Cold sintering process
Bio-active composite
Interfacial bonding
Composite consolidation
Plasticization effect

ABSTRACT

Developing a nanocomposite that combines the stiffness of hydroxyapatite (HA), a bone-mimicking mineral, with the flexibility, and resorbability of polylactic Acid (PLA), a biodegradable polyester, presents significant potential in bone regeneration applications. The cold sintering process (CSP) offers a novel approach for consolidating HA-PLA composite at low temperatures, addressing the co-sintering challenge posed by higher consolidation temperatures requirement for HA compared to PLA's compaction, or extrusion temperatures. This study investigates the effect of HA-to-PLA ratios and the plasticizing effect of PLA on the composite's consolidation behavior and mechanical properties, with a specific focus on HA consolidation within the PLA matrix under CSP conditions at 200 °C under 360 MPa pressure. Interestingly, the results revealed that the HA consolidation in composite matrix changes with PLA content and the plasticizing effect has a crucial role in enhancing this consolidation. An optimal HA-to-PLA weight ratio of 80:20 yielded superior HA consolidation and strong interfacial bonding between HA particles and HA and PLA, achieving an ideal mechanical strength and structural integrity balance. Overall, the HA-PLA composites exhibit mechanical strength comparable to human cortical bone, making them suitable for potential biomedical applications.

## 1. Introduction

Available biomaterial options for treating critical-sized bone defects with infections or trauma-induced segmental bone loss are limited. The gold standard autogenous bone grafts, often become impractical due to the restricted volume of bone that can be safely harvested [1–3]. In some cases, treating such defects becomes even more challenging, especially for older individuals with limited regenerative potential [4]. Recent advancements in biomaterials engineering have shifted focus toward synthetic bone substitutes, particularly inorganic-organic composites as next-generation biomaterials for treating critical-sized bone defects. This logical approach for composite development is inspired by natural bone, which is a composite matrix primarily composed of collagen (organic phase) and apatite crystals (inorganic phase) [1–3]. Thus the current strategies aim to replicate the hierarchical structure and functionality of natural bone by combining the advantages of the strength and stiffness of synthetic bioactive ceramics, and the flexibility and biodegradability of biopolymers. However, developing composites with the necessary mechanical properties for load-bearing sites mostly relies on composite processing techniques.

A diverse array of bioactive ceramics and polymer materials have been explored for bone-regenerative applications. Synthetic nano-hydroxyapatite is the most encountered bioceramics, due to its structural and chemical similarity to the inorganic-mineral phase found in natural bones [5]. In the realm of polymer, polylactic acid, a biodegradable and biocompatible polyester, has gained significant attention for biomedical applications owing to its tailorable degradation rate, high stiffness, and wide processing temperature [6–9]. Poly(L-lactic acid) (PLA) is a semi-crystalline polyester with a $T_m$ close to 180°C and a $T_g$ close to 60°C, that can be readily modulated by copolymerization [10].

---

* Corresponding author at: Laboratory of Polymeric and Composite Materials, Centre of Innovation and Research in Materials and Polymers, University of Mons, Place du Parc 23, Mons 7000, Belgium.
** Corresponding author.
*E-mail addresses:* muthusundark@gmail.com, muthusundar.kumar@umons.ac.be (M. Kumar), jean-marie.raquez@umons.ac.be (J.-M. Raquez).

https://doi.org/10.1016/j.mtcomm.2025.112322
Received 26 November 2024; Received in revised form 7 January 2025; Accepted 22 March 2025

Furthermore, PLA's eco-friendly production from renewable, non-toxic feedstocks like sugarcane and corn starch enhances its suitability for human body applications. It is also classified as "generally recognized as safe" (GRAS) by the FDA [7]. Despite their advantageous features, HA and PLA possess inherent limitations; HA presents an elevated brittleness and PLA lacks bioactivity with low strength [5–7]. Consequently, integrating the beneficial properties of both HA and PLA has garnered significant interest, as their combination overcomes individual limitations, supports bone ingrowth, and facilitates the gradual replacement of implants with new bone tissue [4].

Despite the advantages of HA/PLA composite, achieving mechanical strength comparable to natural bone remains challenging when fabricating them via injection molding or solvent casting. For instance, adding 10–30 wt% of HA to the PLA matrix improves the mechanical properties of final composites, but they remain inferior to the natural bone [11–13]. Many researchers emphasized that the ceramic-to-polymer content and poor interfacial affinity between hydrophilic HA and hydrophobic PLA significantly influence the mechanical strength of the resulting composites. Moreover, the proportion of ceramic and polymer is a critical parameter to achieve composites with excellent mechanical properties [13–17]. However, melt-processing composites with higher ceramic content negatively impact the dispersion and homogeneity of HA within the PLA matrix, resulting in weaker mechanical performances [16,17]. Additionally, this method fails to consolidate the HA particles within the PLA matrix, which is crucial for achieving high strength [18]. HA typically requires high temperature (>1200 °C) for consolidation to enhance its mechanical properties, but it remains brittle. Due to the significant difference in melting temperatures between HA (>1200 °C) and PLA (>150 °C), they cannot be sintered together, making the consolidation of HA with the PLA matrix using conventional composite processing techniques highly complex [19].

Researchers have demonstrated that pressure-assisted consolidation techniques significantly enhance the consolidation of ceramic particles within the polymer matrix, resulting in improved interfacial bonding between the ceramic and polymer. This process also increases the mechanical strength of bioactive composites with a higher ceramic content [18–20]. In this context, a low-energy sintering technique known as the cold sintering process (CSP) is gaining popularity for its simple experimental setup and ability to consolidate various ceramics, including bioceramics such as HA, at low processing temperatures (200–350 °C) under the application of transient liquids and pressures up to 600 MPa [21]. Consequently, the consolidation temperature aligns with the processing temperature of PLA, facilitating the co-integration of HA-PLA into a bioactive composite suitable for bone regenerative application [19,22].

Hu et al. [22], reported the cold sintering of *in-situ* drug-loaded HA-PLA composites proportions at various temperatures (60–120 °C) and pressures (100–700 MPa). Specifically, for the HA/PLA 80/20 wt% composite proportion, they observed that the relative density did not exceed 87 %, even with increasing temperature and pressure [22]. This leaves uncertainty regarding whether the consolidation was primarily dependent on temperature, pressure, or their interplay. Furthermore, the pattern of HA consolidation within the composite remains unclear. Alternatively, Pietrzykowska et al. [18], consolidated the 80/20 wt% HA/PLA composite using various protocols. They found that cold pressing at a pressure of 1 GPa achieved a relative density of up to 85 %. Moreover, a two-step process involving cold axial pressing at 1 GPa followed by hot isostatic pressing at 75 MPa and 165 °C resulted in a relative density of 99 % [18]. In the context of the cold sintering process, a suitable liquid phase is crucial to drive the dissolution-precipitation phenomenon at the particle surface, as several studies, including ours, have demonstrated. Freshly co-precipitated HA can be densified without using any liquid due to the presence of highly adsorbed water molecules [23,24]. Since PLA does not behave like aqueous liquids, the consolidation behavior of HA in HA/PLA composites processed without any liquids remains uncertain. It is important to mention that aqueous liquids cannot be used for HA/PLA composite consolidation, as PLA is an aliphatic polyester and is prone to hydrolytic degradation [25]. However, the fluidity of PLA changes with temperature, and its binding properties can potentially be exploited to consolidate the composites.

The present study explores the consolidation behavior of HA/PLA composites under 360 MPa pressure at 200 °C. Our previous research demonstrated that commercial HA can achieve up to 67 % densification under these conditions without the use of liquids [24]. At 200 °C, HA particles are expected to consolidate, while PLA transitions into a fully viscous state, facilitating the integration of HA and PLA. Special attention is also given to the plasticization effect of PLA in the consolidation of composites, as plasticizers are known to enhance the fluidity, flexibility, and ductility of PLA [26,27]. Tributyl citrate (TBC), a plasticizer with low molecular weight, was selected for its miscibility, biocompatibility, and proven effectiveness in improving PLA fluidity and compatibility with HA [26,27]. This study further examines the interfacial bonding between HA and PLA, the effects of varying HA-to-PLA ratios, and the impact of PLA plasticization. An emphasis was placed on understanding how PLA fluidity influences composite consolidation and mechanical properties.

## 2. Materials and methods

### 2.1. Materials

A commercially available, HA powder (nanoXIM.HAp202, CAS 12167–74–7) was procured from FLUIDINOVA S.A. These stoichiometric HA powders (Ca/P ~ 1.67) contain spherically aggregated nano HA particles ($d_{50}$ =5.0 ± 1 µm, BET specific surface area = 97 $m^2/g$), and the detailed physical and chemical characteristics can be found elsewhere [24]. The PLA with the trade name Ingeo biopolymer PLA 6201D (number-average molar mass ($M_n$) = 1,16,200 g/mol, dispersity (Đ = 2), obtained by Size Exclusion Chromatography (SEC) calibrated with polystyrene (PS) standard in $CHCl_3$, D-isomer < 2 % according to the supplier), was supplied in granule form (between 0.3 and 0.5 mm) by NatureWorks LLC (USA). The solvent chloroform (CAS 67–66–3) from Chemlab analytical and the plasticizer tributyl citrate (CAS 77–94–1) (MW = 360.44 g/mol) from Sigma Aldrich were used as received.

### 2.2. Preparation of HA/PLA composite powder

HA/PLA composite powders at different mass fractions of HA/PLA (50/50, 60/40, 70/30, 80/20 wt%) were prepared via the solvent evaporation method. The schematic illustration of the process involved in the HA/PLA composite powder preparation and its consolidation using the cold sintering setup is shown in the supplementary information Fig. S1. Initially, the PLA was dissolved in chloroform at room temperature in a closed container under continuous magnetic stirring. Then, the required amount of HA powders was dispersed into the PLA solution under stirring for 3 hours. Following this, the container was left open overnight to allow a slow solvent evaporation under mild stirring conditions. The resulting composite solid mass was dried in a hot air oven at 80 °C for 6 hours. The HA:PLA 80:20 wt% powder was obtained in soft powder form without any lumps, while the other samples consisted of solid chucks. The description of composite powder morphology is given in supporting information Fig. S2. The solid lumps were subsequently cryo-milled using a Retsch vibro mill with a ball-to-mass ratio of 30:1. The milling was carried out at a frequency of 30 Hz for 9 min, divided into three cycles of 3 min each, with auto precooling to liquid $N_2$ temperature before each cycle. The prepared composite powders were named based on their compositions: HA:PLA 50:50, 60:40, 70:30, and 80:20.

### 2.3. Cold sintering of HA/PLA powders

Approximately 1 g of the respective HA/PLA powders was filled into a cylindrical steel die (∅ = 13 mm) equipped with a heating jacket and a thermocouple. A 1 mm thick polyimide pellet was used to prevent the PLA adhesion to the die surface. The composite powder underwent pre-pressing under uniaxial compression using a mechanical testing machine (Zwick Roell model Retroline 1185 with a 100 kN load cell) at 360 MPa (7 kN/min head speed) and held for 15 minutes at room temperature. Subsequently, the sample was heated to 200 °C at a rate of 5 °C/min and held at that temperature for 10 min. During the cold sintering process at 360 MPa pressure, changes in the sample's compact volume were recorded as a function of total displacement over time, using the machine's built-in displacement transducer sensor to monitor the consolidation trend throughout the CSP.

### 2.4. Plasticization of PLA and cold sintering

To assess the effect of PLA fluidity, the PLA was plasticized with tributyl citrate at concentrations of 5, 10, and 20 wt% using a DSM micro compounder (15cc chamber with a vertical twin-screw configuration). The PLA was loaded into the preheated chamber at 190 °C, with the screw speed set to 30 rpm during feeding, and 100 rpm during mixing for 3 min. The required amount of TBC was then added and the mixture was compounded for 5 min. The extruded plasticized PLA was collected and allowed to solidify at room temperature. Subsequently, the HA:PLA 80:20 wt% composite powder was prepared with the plasticized PLA and cold sintered using the previously discussed protocols. The resulting composite powders were designated as HA:5TBC/PLA, HA:10TBC/PLA, and HA:20TBC/PLA, corresponding to the different TBC concentrations.

### 2.5. Characterizations

The bulk density of the cold-sintered and compacted samples was calculated by measuring mass and geometric dimensions. At least three samples of each composition were considered and the bulk density was calculated using the following relation (1),

$$R = 4m/\left(\pi d^2 h\rho\right) \times 100 \tag{1}$$

where R is the relative density, $m$ is the mass, $d$ is the diameter, $h$ is the thickness, and $\rho$ is the theoretical density. The theoretical density was calculated using the relation 2,

$$\rho = \frac{m}{\left(m_{HA}/\rho_{HA} + m_{PLA}/\rho_{PLA}\right)} \tag{2}$$

where $m_{\mathrm{HA}}$ and $m_{\mathrm{PLA}}$ represent the masses of HA and PLA in the composite, while $\rho_{\mathrm{HA}}$ and $\rho_{\mathrm{PLA}}$ represent the theoretical density of HA and PLA respectively. The measured true density of 2.96 g/cm$^3$ for HA (Helium pycnometer Accypyc III (Micro-meritics, USA)), and 1.24 g/cm$^3$ for PLA (provided by the supplier) were used in the calculations. For the composite made with plasticized PLA, the measured density of the PLA, based on the Archimedes principle (mass/volume), was used in the bulk density calculation. The samples 5TBC/PLA and 10TBC/PLA had densities of 1.24 g/cm$^3$ , while 20TBC/PLA had a 1.22 g/cm$^3$ density.

The phase composition of the cold-sintered composites was characterized using a Panalytical X'Pert Pro diffractometer, equipped with Cu Kα radiation (λCu = 1.542 Å) operating at 40 kV and 40 mA. Diffraction patterns were recorded over a 2θ angle range of 10° to 40°, with a scan step size of 0.013°. The microstructure of the cold-sintered samples, including cross-sections of samples containing 20 and 30 wt% PLA, was examined using a GAIA 3 TESCAN field emission scanning electron microscope (FE-SEM) equipped with a Ga-focused ion beam (COBRA column) to prepare the cross-sections of the specimens.

The chemical bonding characteristics of the composites were assessed through Fourier transform infrared (FTIR) analysis using a Bruker IFS 66 V/S spectrometer in ATR-FTIR mode. The spectra were recorded over the wavenumber range of 4000–530 cm$^{-1}$ in transmittance mode, with a resolution of 4 cm$^{-1}$ . Micro-indentation analysis was performed using a Zwick Roell (ZHU 0.2) micro-hardness tester equipped with a Vickers diamond indenter. Indentations were made after polishing the sample surface (up to 2400 grit), with a load of 20 N applied for 13 seconds at a constant displacement rate of 20 N/min during the loading-unloading cycle. The reduced elastic modulus was calculated from the unloading load-displacement data using the Oliver-Pharr method [28]. 10 random indents were made on each sample, and two samples were tested for each composition. The average values of the elastic modulus and Vickers hardness are presented.

The thermal behavior of the cold-sintered composite samples and plasticized PLA was analyzed using the TA Q2000 model differential scanning calorimeter. Approximately 8–9 mg of each sample was used for experiments under a nitrogen atmosphere (50 mL/min). The experiments were conducted over a temperature range of −80 °C to 200 °C, including an initial heating cycle to 200 °C, followed by cooling to −80 °C, and then a second heating cycle to 200 °C, all at a heating/cooling rate of 10 °C/min. The glass transition temperature ($T_g$), crystallization temperature ($T_c$), and melting temperature ($T_m$) of the PLA and composites were determined from the second heating curve.

## 3. Results and discussions

### 3.1. Consolidation of HA/PLA

The extent of consolidation and the influence of HA-to-PLA content on the microstructure and density evolution during the CSP is illustrated by the compact volume shrinkage profile shown in Fig. 1(b). The inset dotted lines of Fig. 1(b) indicate the heating program during the CSP at 360 MPa. Overall, when comparing the compact volume changes reflected by the displacement over time for the composite samples (Fig. 1 (b)), the order follows: HA:PLA 80:20 > 70:30 > 60:40 > 50:50. However, the relative density exhibits an opposite trend, suggesting differences in the microstructure as well as the consolidation pattern between HA and PLA.

During the initial compaction phase at room temperature for 15 minutes, HA particles undergo elastic deformation, while PLA particles experience viscous deformation. This process causes a rearrangement of HA and PLA particles into a compact, dense structure, thereby reducing porosity [29,30]. This allows the compact to achieve a relative density of more than 80 % (Fig. 1(a)). However, the extent of elastic deformation of HA particles within the compact varies depending on the HA-to-PLA ratio. Increasing PLA content within the compact restricts the elastic deformation of HA particles compared to lower PLA content, as indicated by the differences in volume changes shown in Fig. 1(b). At this stage, the variation in relative density values of the compacted samples (Fig. 1(a)) suggests that lower PLA content facilitates greater interparticle bonding between HA particles, despite higher porosity. Conversely, increasing the PLA proportion reduces porosity by filling voids, as the PLA adheres to HA particles under the compaction effect [29–31].

During the heating phase up to 200°C at a 5 °C/min ramp rate, two instances of negative volume shrinkage were observed between 30–50°C and above 140°C due to the thermal expansion of PLA. The first negative shrinkage (30–50°C) arises from the release of internal stress as the rigid PLA chains transition into a less dense, flexible form [32,33]. This transformation promotes the elastic deformation of HA particles caused by the viscous flow of PLA within the compact, as reflected by the volume shrinkage up to 140°C. Between 140°C and 200°C, the softened PLA gradually transitions into a flowable state, accompanied by volume relaxation of the polymer chains, which contributes to the second negative volume shrinkage (Fig. 1(a)) [32,33]. This process may induce strong repulsion at the interphase, likely due to polarity differences or thermal expansion mismatches between HA and PLA [32]. During the

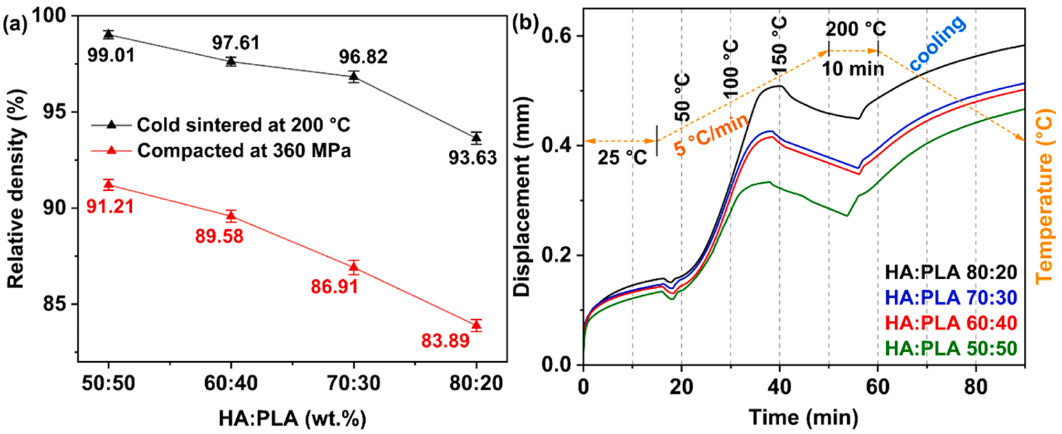

**Fig. 1.** (a) Relative density values of the compacted and cold sintered samples, (b) volume shrinkage profile of the compact recorded in terms of total displacement versus time during the cold sintering of composite under 360 MPa.

10-minute holding period at 200°C, PLA remains in a flowable state, allowing for viscoelastic deformation during the subsequent cooling stage. This state facilitates further bonding with HA particles and fills any voids, thereby enhancing composite consolidation. However, the flowability or fluidity of PLA may vary with HA content, resulting in different consolidation patterns between HA and PLA. Additionally, the composite's consolidation mechanism is considerably more complex compared to the consolidation of pure HA powders under similar conditions.

In our previous study on the cold sintering of the same HA powder used in this research at 200 °C without any liquids, the volume shrinkage profile (Fig. S3, left) indicates that consolidation occurs primarily through particle rearrangement driven by the elastic deformation of HA particles. During heating, the volume shrinkage is further influenced by viscous flow, which is triggered by precipitation-recrystallization reactions across the grain contact points (grain boundaries), facilitated by adsorbed water molecules in HA powder. This process ultimately supports the consolidation of HA, resulting in a microstructure composed of well-bonded nanograins (Fig. S3) with a relative density of 66 % [24]. However, this consolidation trend cannot be directly compared to the volume changes observed during the cold sintering of the HA:PLA composite. In the composite, the presence of PLA may influence the contact between HA grains or particles, introducing uncertainty in the comparison.

The differences in the observed consolidation and relative density trends can be commented on relating to the microstructure of the composite samples illustrated in Fig. 2. As seen in Fig. 2($b_1$ to $d_1$), the mechanical interlocking between PLA and the HA aggregates becomes more pronounced with an increasing PLA content [30,31]. Additionally, Fig. 2($b_2$-$d_2$) shows evidence of PLA infiltration into the interparticle gaps of the HA aggregates. In these cases, the increased PLA content hinders the breakdown of HA aggregates and affects their dense packing within the PLA matrix (Fig. 2($b_1$ to $d_1$)). As a result, the consolidation of HA grains, as observed in Fig. S3, becomes less feasible with higher PLA content. Instead, cold sintering primarily facilitates consolidation between HA aggregates and PLA, where PLA forms a uniform matrix that binds the HA aggregates, likely contributing to higher relative densities. In contrast, the microstructure of HA:PLA 80:20 sample (Fig. 2($a_1$&$a_2$))

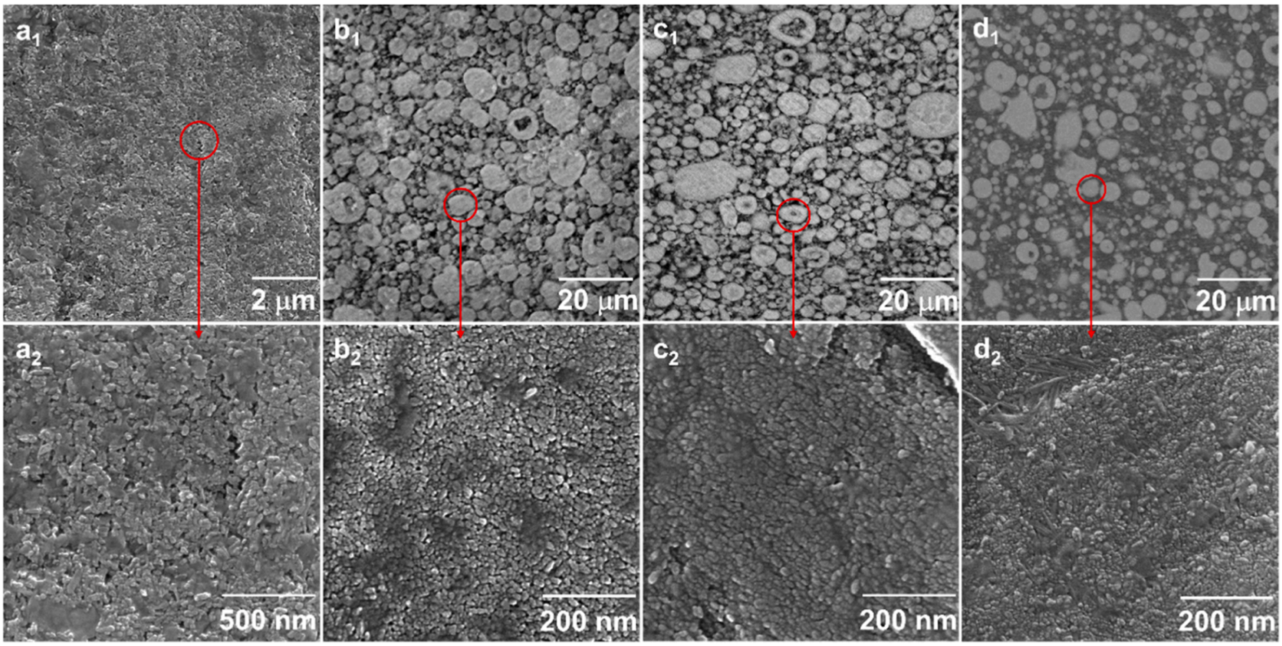

**Fig. 2.** Cold sintered composites microstructure (polished surface); ($a_1$&$a_2$) 80:20 fraction captured in SE mode at magnification 110Kx & 150Kx, ($b_1$-$d_1$) and ($b_2$-$d_2$) corresponds to 70:30, 60:40 and 50:50 fractions captured in BSE mode at magnification 2Kx and in SE mode at 150Kx magnification respectively.

consists of well-consolidated nano HA grains with PLA homogeneously binding the inter-particle matrix grains. The packing of HA grains in the microstructure of the HA:PLA 80:20 sample is comparable to that of cold-sintered HA (Fig. S3). This suggests that the low PLA content (20 wt %) appears to facilitate the de-aggregation of HA aggregates into individual nanograins, promoting the consolidation of HA grains while PLA hierarchically binds them [29]. However, the dynamics of HA grain consolidation within the composite matrix remain uncertain. Advanced characterization techniques, particularly in-situ X-ray scattering analysis, could provide deeper insights into these mechanisms [37].

Overall a different pattern of consolidation was observed depending on the HA-to-PLA content during the cold sintering. Additionally, the FIB cross-sectioned SEM images in Fig. S4 supported our statements. It reveals that the cold sintered sample HA:PLA 80:20 has a continuous nano HA grain matrix, while the HA:PLA 70:30 sample shows a densely packed HA aggregate as it is surrounded by more PLA matrix.

### *3.2. Plasticization effect on consolidation of HA/PLA*

Plasticizers are widely recognized for enhancing the compatibility between the hydrophilic HA and hydrophobic PLA by improving the mobility of PLA chains [26]. The DSC curves of PLA plasticized with different TBC concentrations are presented in Fig. 3(a), and the summarized values of the thermal properties are given in supporting information Table S1. The changes in the $T_c$, and $T_m$ of the plasticized PLA indicate that TBC partially disrupts the crystalline regions of PLA. As the TBC concentration increases, the $T_g$ shifts to lower temperatures, confirming that plasticization enhances the mobility of PLA chains [34,35]. Since the PLA used in this study is semi-crystalline, plasticization not only helps to improve the fluidity of PLA but is also expected to facilitate better interaction between HA and PLA [35].

The influence of plasticization on the consolidation behavior during CSP was tested with the 80:20 fraction of HA:PLA, where the HA de-aggregation is significant (see Fig. 2(a)$_1$&a$_2$). Comparing the volume shrinkage profile shown in Fig. 3(b) for the HA:TBC/PLA 80:20 composites and HA:PLA 80:20 composite, the consolidation pattern for composites made with plasticized PLA is the same as the unplasticized PLA. The elastic deformation at the initial compaction phase i.e., at room temperature is similar to those made with unplasticized PLA (HA: PLA 80:20). However, due to the enhanced fluidity of plasticized PLA, a visible difference in the viscoelastic deformation is observed near heating up to 140 °C. Moreover, as shown in Fig. 3(c), the relative density values of the plasticized PLA composites are improved with increasing TBC concentration and are higher compared to the unplasticized PLA composite. Further, by comparing the microstructure of 80:20 composite made with unplasticized (Fig. 2(a$_1$&a$_2$)) and 20TBC plasticized PLA shown in Fig. 4, we can observe a significant improvement in the dense packing of nano HA grains bonded with PLA. Thus, plasticization positively impacts both the overall composite consolidation and the consolidation of HA within the composite matrix. This strongly emphasizes that the consolidation in the composite during cold sintering is significantly influenced by the fluidity of PLA.

### *3.3. HA consolidation extent in the composite matrix*

The consolidation behavior of HA within the composite matrix can be demonstrated by the ability to recover the HA matrix after extracting PLA from the composite matrix. The PLA was extracted from the cold

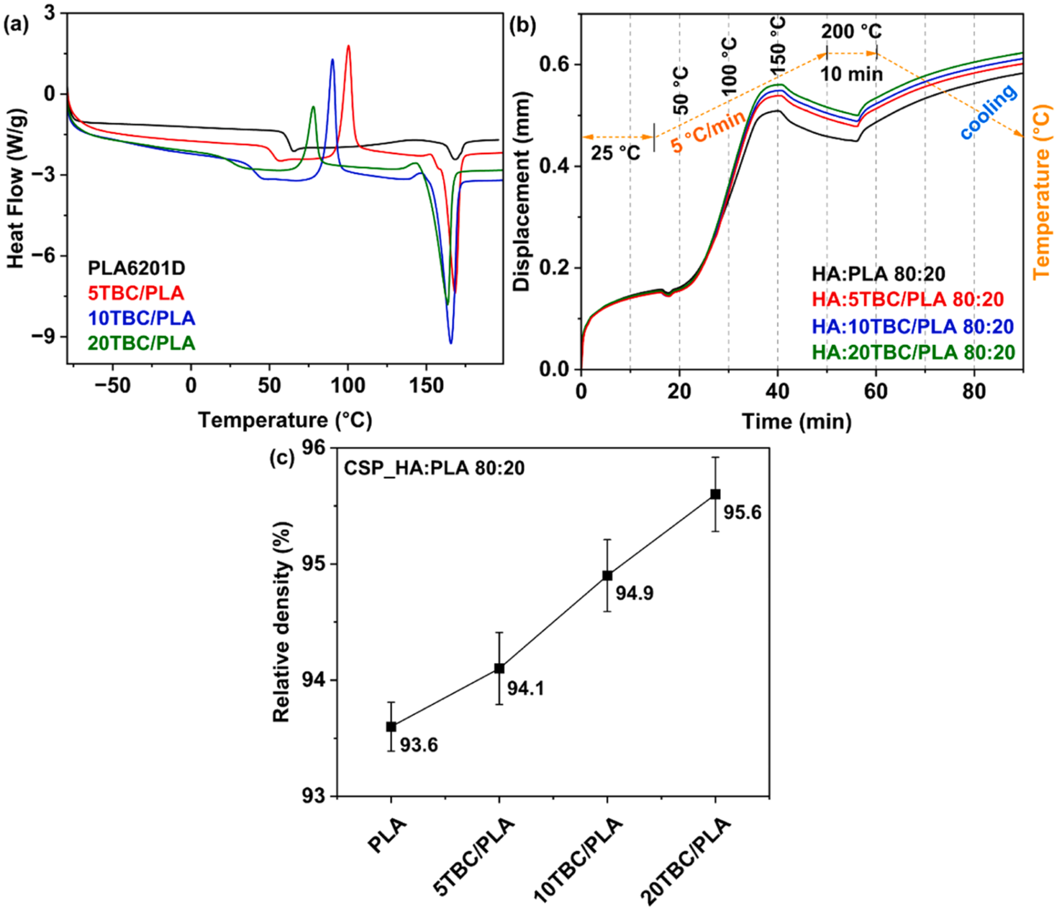

**Fig. 3.** (a) DSC thermograms of the TBC plasticized PLA, (b) volume shrinkage profile of the compact recorded in terms of total displacement versus time during the cold sintering of composite made with plasticized PLA under 360 MPa, and (c) Relative density values of the cold sintered composites made with plasticized PLA.

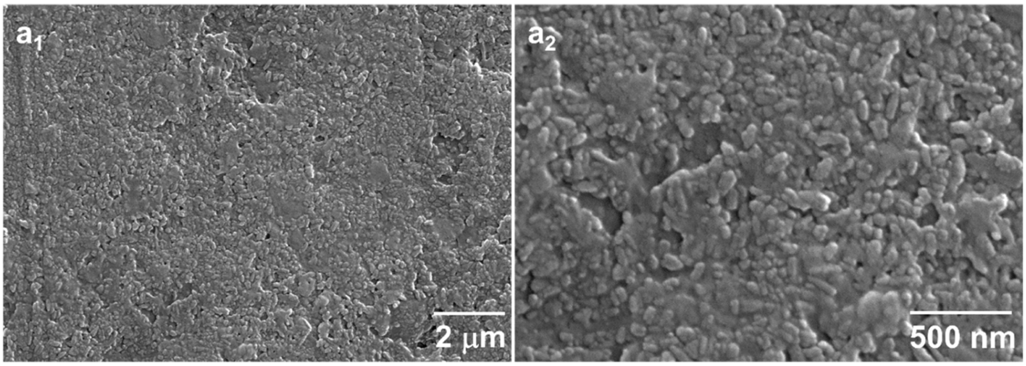

**Fig. 4.** ($a_1$&$a_2$) Microstructure of the cold sintered composite (polished surface); HA:20TBC/PLA 80:20 fraction captured in SE mode at magnification of 110Kx & 150Kx.

sintered samples HA:PLA 80:20, 70:30, 60:40, 50:50, and HA:20TBC/PLA, by the Soxhlet extraction method using chloroform, as it serves as PLA's good solvent. After 24 hours of extraction, the HA matrix was retrieved (shown in Fig. S5) only for the sample with an 80:20 proportion indicating that the nano HA gains are successfully consolidated. Complete extraction of PLA from the composite matrix was confirmed by a weight change of 19.2 % after drying at 100 °C. In contrast, the other compositions only yielded the HA powders. This implies that the 80:20 ratio promotes HA consolidation within the composite, providing structural integrity along with PLA bonding. The same observation was also found with HA:20TBC/PLA composite. Further to evaluate the impact of plasticization on the extent of HA consolidation after PLA extraction, SEM analysis along with specific surface area (SSA) determination was carried out for the retrieved HA matrix from both plasticized (20TBC) and unplasticized 80:20 composite samples. From Fig. 5, it is confirmed that the HA matrix of both samples constitutes loosely bonded nanograins and has different SSA values (inset value in Fig. 5). Comparing the SSA values of these samples, the grain packing is denser for the composite made of plasticized PLA. From our previous study, in which we investigated the cold-sintering of pure HA without the use of liquids under the same conditions, we observed that the microsite consists of well-bonded nanograins with a relative density of 66 % and an SSA reduced to 33 $m^2/g$ (Fig. S3) after consolidation [24]. In general, densification progresses with mass transfer across grain boundaries and a reduction in surface area/energy [36]. In the case of HA-PLA composite, PLA likely hinders the consolidation dynamics of HA in the composite matrix. During cold sintering, PLA may partially shield the direct grain-to-grain contact that impedes incomplete mass transfer across HA nanograins. As a result, the HA grains within the composite are cohesively bonded but are not as dense as observed in the cold sintering of pure HA [24]. Interestingly, the plasticizing effect contributes to a more cohesive consolidation of HA nanograins within the composite matrix due to the increased flexibility of PLA with a high content of TBC. However, a solid understanding of the cold sintering dynamics of HA grains within the composite matrix should be further validated through advanced characterization techniques, particularly in-situ x-ray scattering analysis [37].

### *3.4. Phase composition and thermal behavior*

PLA6202D, being a semi-crystalline polymer with very low D-isomer content (<2 %) is easily crystallizable [38]. However, the cold-sintering temperature, integration pattern between the HA and PLA, and plasticization are known to influence the crystallization ability of PLA. Typically, PLA crystallizes into ordered α and α′ disordered polymorphs, depending on the crystallization temperature, as extensively discussed in the literature [38,39]. The DSC thermogram of the cold-sintered HA:PLA 80:20 composite fraction made with unplasticized and 20TBC plasticized PLA is shown in Fig. 6(a). The $T_g$ of both the unplasticized (48.2 °C) and plasticized (39.6 °C) composite is significantly lower than the $T_g$ of pure PLA (62.4 °C). This can be attributed to the restricted chain mobility due to improved interactions between HA particles and PLA. These interactions, likely involve hydrogen bonding or mechanical interlocking [30,31]. The existence of hydrogen bonding between HA and PLA was evidenced by the red-shift of the characteristic vibration peak for PLA6201D at 1748 $cm^{-1}$ , corresponding to C═O stretching, as shown in the FTIR spectrum in Fig. 6(c) [22,40]. Moreover, the $T_m$ shifts from 168.7°C for pure PLA to lower values in the composites. In both the composites, the $T_m$ appears broader, indicating a disrupted crystalline structure caused by the nucleating effect of HA. Furthermore, the difference in $T_m$ between the plasticized (161.5 °C) and unplasticized (159.4°C) composites suggests that the plasticization enhances the degree of crystallization or improves the molecular arrangement of PLA [38,39]. These observations are further supported by the XRD patterns

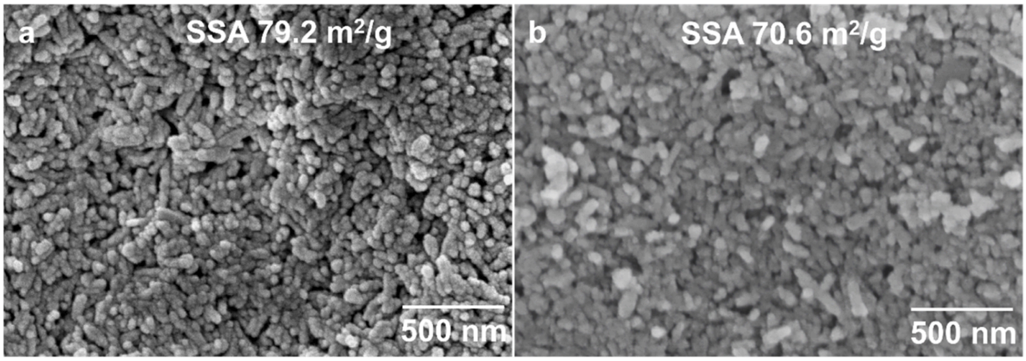

**Fig. 5.** Microstructure of the HA matrix after extracting the PLA from cold sintered (a) HA:PLA 80:20 and (b) HA:20TBC/PLA 80:20 composite. The SEM images were captured in SE mode at a magnification of 150Kx.

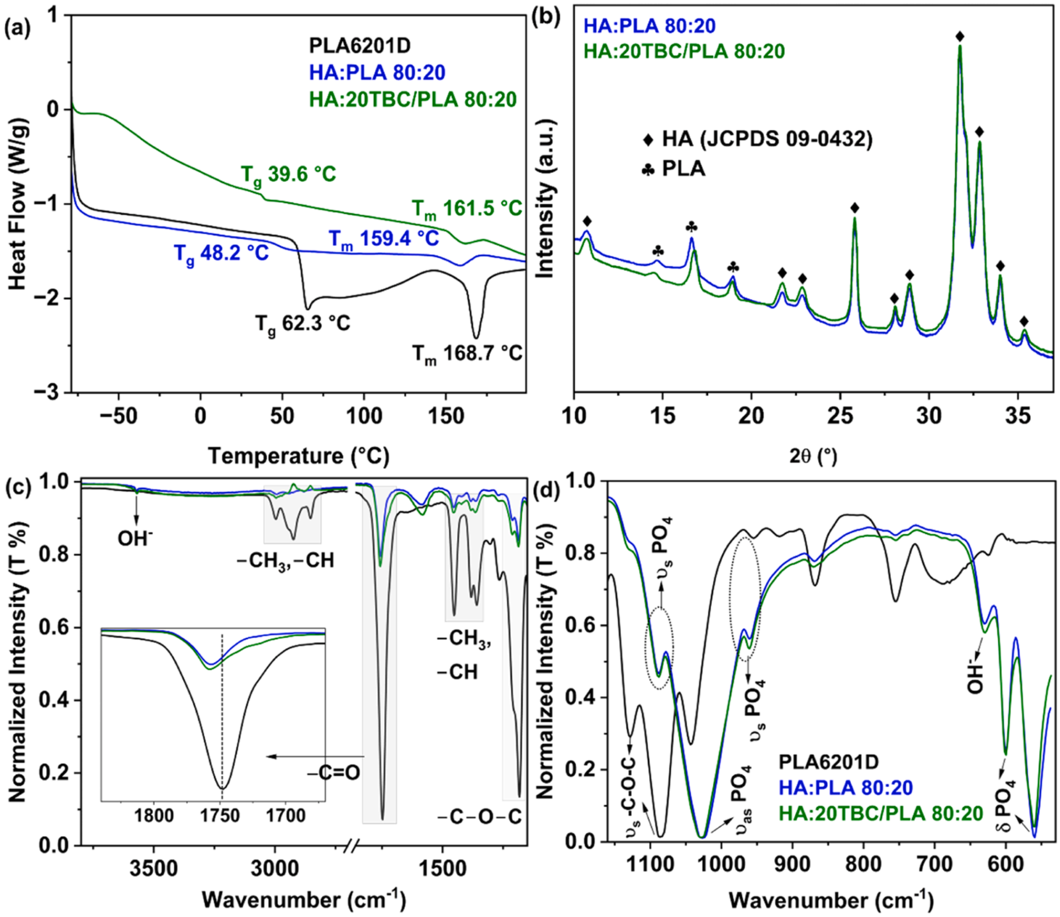

**Fig. 6.** (a) DSC thermogram (b) XRD patterns and (c and d) FTIR plot of the HA:PLA 80:20 composite made with unplasticized and 20TBC-plasticized PLA.

illustrated in Fig. 6(a). The XRD results indicated that the cold-sintered composites have HA and PLA phases. The diffraction peaks corresponding to the HA crystal phase align with the JCPDS 00–009–0432 pattern. Both the composite shows the diffraction peaks at 2θ = 14.7, 16.6, and 18.9° correspond to (010), (110)/(200), and (203) lattice planes of the α/α′ crystal forms of PLA [38,39]. The heterogeneity in the crystal form of PLA, attributed to the nucleation effect of HA, is further evidenced by the FTIR bands at 755 and 867 cm$^{-1}$ (Fig. 6(d)) [41]. While comparing the unplasticized composite, the diffraction peak at 16.6° in the plasticized composite slightly shifts to 16.8°, accompanied by a minor increase in intensity. This shift suggests that plasticization enhances the PLA crystallization during the cold sintering process [42].

The crystallization behavior of PLA in the composite varies (Fig. S6 (a)) due to the differences in the consolidation pattern between hydroxyapatite (HA) and PLA, as shown in Fig. 2, with increasing PLA content. Additionally, these composites exhibit similar phase characteristics and H-bonding between HA and PLA, which are discussed in detail in the supporting information (Fig. S6).

### 3.5. Mechanical characteristics of the composites

The micro-indentation analysis reveals significant insights into the mechanical interfacial bonding between HA and PLA in cold-sintered composites. As illustrated in Fig. 7(a), the 80:20 HA-PLA composite

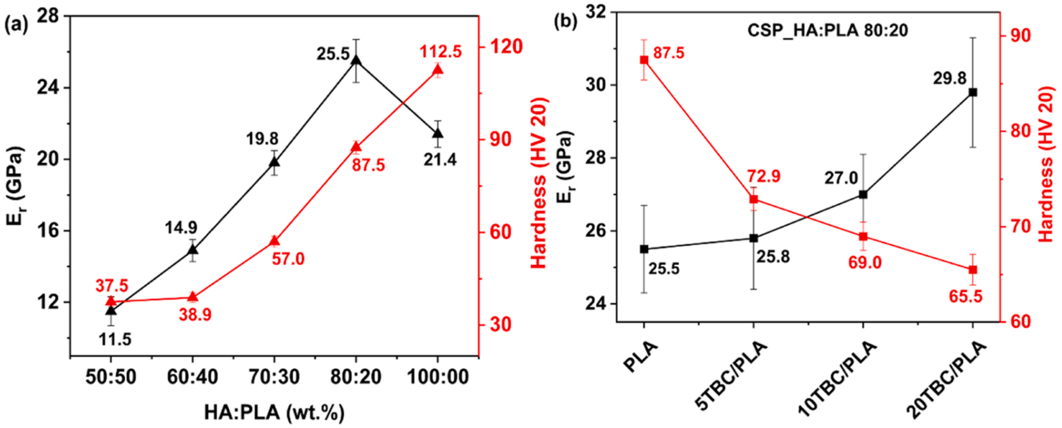

**Fig. 7.** Stiffness/hardness values (a) for the cold sintered composites made with unplasticized PLA and (b) 80:20 composite made with TBC-plasticized PLA.

exhibits the highest elastic modulus ($E_r$ = 25 GPa) and superior hardness, outperforming other composite compositions. In comparison, pure HA cold-sintered under the same conditions (RD 66 %) shows a slightly lower elastic modulus ($E_r$ = 21 GPa) but a higher hardness (112 HV), indicating that the PLA addition improves elasticity but reduces hardness due to the integration of flexible polymer matrix. PLA, being a soft material with low stiffness and hardness, the increasing proportion of PLA in composites reduces the hardness and $E_r$ values relative to HA. However, the lower PLA content (20 %) provides optimal mechanical performance, due to the cohesive consolidation of HA nanograins (Fig. 5(a)) within the matrix facilitated by PLA's binding effect. Similarly, when TBC plasticized PLA was used in 80:20 composites, the stiffness increased with higher TBC content, while hardness decreased (Fig. 7(b)). The increase in stiffness is attributed to the plasticization effect, which enhances the cohesive consolidation of HA grains (Fig. 5(b)) within the composite matrix. The lowering of hardness values suggests that the plasticization strengthens and softens the PLA, as indicated by the DSC profile (Fig. 6(a)) [35]. As HA primarily provides stiffness, the consolidation of HA in the composite matrix contributes higher stiffness values for HA:PLA 80:20 proportion composites, offering excellent structural integrity through the combined effect of binding between PLA and HA. The microstructural observations and the results in Section 3.3 together support this conclusion. Overall, the obtained stiffness values are comparable to the stiffness value of human cortical bone reported in the literature [43,44]. The composite processed through the cold-sintering process is therefore suitable for bone substitutes at load-bearing sites.

## 4. Conclusions

This study offers new insights into the consolidation behavior during the cold sintering of HA-PLA composites at 200°C under 360 MPa pressure. Cold sintering processing (CSP) facilitates the creation of high-strength composites with a relative density exceeding 90 %, effectively combining HA's stiffness with PLA's flexibility. The consolidation pattern between HA and PLA, as well as the consolidation of HA grains within the composite matrix, depends significantly on the HA-to-PLA ratio and the fluidity of PLA. Higher PLA content increases the overall density of the composite, as consolidation primarily occurs between HA aggregates and PLA. In contrast, lower PLA content promotes the consolidation of HA grains within the matrix, as well as between HA grains and PLA. In particular, the HA:PLA ratio of 80:20 demonstrates superior mechanical properties due to the strong cohesive consolidation between HA grains and the mechanical interlocking between HA and PLA. Plasticization plays a key role in enhancing the crystallization of PLA during cold sintering, thereby improving the consolidation of HA grains and strengthening the interaction between the well-crystallized PLA and HA. This leads to a stiffer composite structure, although the plasticizer introduces some flexibility, resulting in reduced hardness compared to the unplasticized composite. The cohesive consolidation of HA nanograins and the binding effect between HA and PLA create a strong chemical and mechanical interphase. While cold sintering successfully integrates HA and PLA through strong interfacial and chemical bonds, the HA-HA bonding remains critical for providing the necessary stiffness in the composite structure.

## CRediT authorship contribution statement

**Leriche Anne:** Writing – review & editing, Validation, Supervision, Funding acquisition, Conceptualization. **Raquez Jean-Marie:** Writing – review & editing, Validation, Supervision, Resources, Funding acquisition, Conceptualization. **Lasgorceix Marie:** Validation, Supervision, Resources, Conceptualization. **Mincheva Rosica:** Validation, Supervision, Resources, Conceptualization. **Ben Achour Mohamed Aymen:** Validation, Supervision, Resources, Methodology, Conceptualization. **Ölmez Vedi:** Writing – review & editing, Resources, Formal analysis. **Kumar Muthusundar:** Writing – original draft, Visualization, Validation, Methodology, Investigation, Formal analysis, Data curation, Conceptualization.

## Declaration of Competing Interest

The authors declare that they have no known competing financial interests or personal relationships that could have appeared to influence the work reported in this paper.

## Acknowledgments

The authors wish to thank the Wallonia-Brussels Federation, Campus France, and the EUNICE (European University for Customized Education) for general support in the framework of a joint PhD project between UMONS and UPHF. J.M. Raquez is a FRS-FNRS senior research associate. M. Kumar was so thankful to Dr. Florian Jean and Mr Benoit Jorgowski for their assistance in SEM characterization.

## Appendix A. Supporting information

Supplementary data associated with this article can be found in the online version at doi:10.1016/j.mtcomm.2025.112322.

## Data Availability

Data will be made available on request.

## References

[1] R.M. Raftery, I.M. Castaño, G. Chen, B. Cavanagh, B. Quinn, C.M. Curtin, S. A. Cryan, F.J. O'Brien, Translating the role of osteogenic-angiogenic coupling in bone formation: highly efficient chitosan-pDNA activated scaffolds can accelerate bone regeneration in critical-sized bone defects, Biomater 149 (2017) 116–127, https://doi.org/10.1016/j.biomaterials.2017.09.036.

[2] S. Verrier, M. Alini, E. Alsberg, S.R. Buchman, D. Kelly, M.W. Laschke, M. D. Menger, W.L. Murphy, J.P. Stegemann, M. Schütz, T. Miclau, Tissue engineering and regenerative approaches to improving the healing of large bone defects, Eur. Cell Mater. 32 (2016) 87–110, https://doi.org/10.22203/ecm.v032a06.

[3] J. Russias, E. Saiz, R.K. Nalla, K. Gryn, R.O. Ritchie, A.P. Tomsia, Fabrication and mechanical properties of PLA/HA composites: a study of in vitro degradation, Mater. Sci. Eng. C. 26 (2006) 1289–1295, https://doi.org/10.1016/j.msec.2005.08.004.

[4] B.D. Sui, C.H. Hu, A.Q. Liu, C.X. Zheng, K. Xuan, Y. Jin, Stem cell-based bone regeneration in diseased microenvironments: challenges and solutions, Biomater 196 (2019) 18–30, https://doi.org/10.1016/j.biomaterials.2017.10.046.

[5] E. Fiume, G. Magnaterra, A. Rahdar, E. Verne, F. Baino, Hydroxyapatite for biomedical applications: a short overview, Ceramics 4 (2021) 542–563, https://doi.org/10.3390/ceramics4040039.

[6] J.M. Raquez, Y. Habibi, M. Murariu, P. Dubois, Polylactide (PLA)-based nanocomposites, Prog. Polym. Sci. 38 (2013) 1504–1542, https://doi.org/10.1016/j.progpolymsci.2013.05.014.

[7] L. Sha, Z. Chen, Z. Chen, A. Zhang, Z. Yang, Polylactic acid based nanocomposites: promising safe and biodegradable materials in the biomedical field, Int. J. Polym. Sci. 2016 (2016) 6869154, https://doi.org/10.1155/2016/6869154.

[8] H. Lee, D.Y. Shin, Y. Na, G. Han, J. Kim, N. Kim, S.J. Bang, H.S. Kang, S. Oh, C. B. Yoon, J. Park, Antibacterial PLA/Mg composite with enhanced mechanical and biological performance for biodegradable orthopedic implants, Biomater. Adv. 152 (2023) 213523, https://doi.org/10.1016/j.bioadv.2023.213523.

[9] H. Lee, D.Y. Shin, S.J. Bang, G. Han, Y. Na, H.S. Kang, S. Oh, C.B. Yoon, S. Vijayavenkataraman, J. Song, H.E. Kim, A strategy for enhancing bioactivity and osseointegration with antibacterial effect by incorporating magnesium in polylactic acid based biodegradable orthopedic implant, Int. J. Biol. Macromol. 254 (2024) 127797, https://doi.org/10.1016/j.ijbiomac.2023.127797.

[10] L. Feng, B. Zhang, X. Bian, G. Li, Z. Chen, X. Chen, Thermal properties of polylactides with different stereoisomers of lactides used as comonomers, Macromolecules 50 (2017) 6064–6073. ⟨https://pubs.acs.org/doi/abs/10.1021/acs.macromol.7b00818⟩.

[11] H. Sun, M. Ai, S. Zhu, X. Jia, Q. Cai, X. Yang, Polylactide–hydroxyapatite nanocomposites with highly improved interfacial adhesion via mussel-inspired polydopamine surface modification, RSC Adv. 5 (2015) 95631–95642, https://doi.org/10.1039/C5RA21010K.

[12] J. Ferri, M.J. Jordá, N. Montanes, O. Fenollar, R. Balart, Manufacturing and characterization of poly (lactic acid) composites with hydroxyapatite, J. Thermoplas. Compos. Mater. 31 (2018) 865–881, https://doi.org/10.1177/0892705717729014.

[13] S.S. Homaeigohar, A.Yari Sadi, J. Javadpour, A. Khavandi, The effect of reinforcement volume fraction and particle size on the mechanical properties of β-tricalcium phosphate–high density polyethylene composites, J. Eur. Ceram. Soc. 26 (2006) 273–278, https://doi.org/10.1016/j.jeurceramsoc.2004.10.003.

[14] M. Supova, Problem of hydroxyapatite dispersion in polymer matrices: a review, J. Mater. Sci.: Mater. Med. 20 (2009) 1201–1213, https://doi.org/10.1007/s10856-009-3696-2.

[15] X. Carette, L. Dhond, A. Hemberg, D. Thiry, R. Mincheva, J. Cailloux, O. Santana Perez, D. Cossement, M. Dubus, H. Kerdjoudj, R. Snyders, Innovative one-shot paradigm to tune filler–polymer matrix interface properties by plasma polymer coating in osteosynthesis applications, ACS Appl. Bio Mater. 4 (2021) 3067–3078, https://doi.org/10.1021/acsabm.0c01429.

[16] K. Konopka, A. Boczkowska, K. Batorski, M. Szafran, K.J. Kurzydłowski, Microstructure and properties of novel ceramic–polymer composites, Mater. Lett. 58 (2004) 3857–3862, https://doi.org/10.1016/j.matlet.2004.07.025.

[17] J.J. Fallon, S.M. McKnight, M.J. Bortner, Highly loaded fiber filled polymers for material extrusion: A review of current understanding, Addit. Manuf. 30 (2019) 100810, https://doi.org/10.1016/j.addma.2019.100810.

[18] E. Pietrzykowska, B. Romelczyk-Baishya, J. Wojnarowicz, M. Sokolova, K. Szlazak, W. Swieszkowski, J. Locs, W. Lojkowski, Preparation of a ceramic matrix composite made of hydroxyapatite nanoparticles and polylactic acid by consolidation of composite granules, Nanomater 10 (2020) 1060, https://doi.org/10.3390/nano10061060.

[19] N. Guo, H.Z. Shen, P. Shen, Cold sintering of chitosan/hydroxyapatite composites, Materialia 21 (2022) 101294, https://doi.org/10.1016/j.mtla.2021.101294.

[20] F. Brouillet, D. Laurencin, D. Grossin, C. Drouet, C. Estournes, G. Chevallier, C. Rey, Biomimetic apatite-based composite materials obtained by spark plasma sintering (SPS): physicochemical and mechanical characterizations, J. Mater. Sci. Mater. Med. 26 (2015) 1–11, https://doi.org/10.1007/s10856-015-5553-9.

[21] H. Guo, J. Guo, A. Baker, C.A. Randall, Hydrothermal-assisted cold sintering process: a new guidance for low-temperature ceramic sintering, ACS Appl. Mater. Interfaces 8 (2016) 20909–20915, https://doi.org/10.1021/acsami.6b07481.

[22] Y. Hu, D. Xia, H. Shen, J. Nan, N. Ma, Z. Guo, X. Wang, Q. Jin, Cold sintering constructed in situ drug-loaded high strength HA-PLA composites: potential bone substitution material, Ceram. Int. 49 (2023) 11655–11663, https://doi.org/10.1016/j.ceramint.2022.12.014.

[23] H.Z. Shen, N. Guo, L. Zhao, P. Shen, Role of ion substitution and lattice water in the densification of cold-sintered hydroxyapatite, Scr. Mater. 177 (2020) 141–145, https://doi.org/10.1016/j.scriptamat.2019.10.024.

[24] M. Kumar, M.A.B. Achour, M. Lasgorceix, P. Quadros, R. Mincheva, J.M. Raquez, A. Leriche, Densification of hydroxyapatite through cold sintering process: role of liquid phase chemistry and physical characteristic of HA powder, Open Ceram. 17 (2024) 100566, https://doi.org/10.1016/j.oceram.2024.100566.

[25] M.A. Elsawy, K.H. Kim, J.W. Park, A. Deep, Hydrolytic degradation of polylactic acid (PLA) and its composites, Renew. Sustain. Energy Rev. 79 (2017) 1346–1352, https://doi.org/10.1016/j.rser.2017.05.143.

[26] Y. Lemmouchi, M. Murariu, A.M.Dos Santos, A.J. Amass, E. Schacht, P. Dubois, Plasticization of poly (lactide) with blends of tributyl citrate and low molecular weight poly (d, l-lactide)-b-poly (ethylene glycol) copolymers, Eur. Polym. J. 45 (2009) 2839–2848, https://doi.org/10.1016/j.eurpolymj.2009.07.006.

[27] N. Ljungberg, B. Wesslen, Tributyl citrate oligomers as plasticizers for poly (lactic acid): thermo-mechanical film properties and aging, Polymer 44 (2003) 7679–7688, https://doi.org/10.1016/j.polymer.2003.09.055.

[28] G.M. Pharr, W.C. Oliver, F.R. Brotzen, On the generality of the relationship among contact stiffness, contact area, and elastic modulus during indentation, J. Mater. Res. 7 (1992) 613–617, https://doi.org/10.1557/JMR.1992.0613.

[29] A.H. Muhanna, T.Z. Blazynski, Implosive consolidation of polymer ceramic powder composites, Compos. Sci. Technol. 33 (1988) 121–133, https://doi.org/10.1016/0266-3538(88)90014-0.

[30] M. Younesi, M.E. Bahrololoom, Effect of temperature and pressure of hot pressing on the mechanical properties of PP–HA bio-composites, Mater. Des. 30 (2009) 3482–3488, https://doi.org/10.1016/j.matdes.2009.03.011.

[31] N. Ignjatovic, E. Suljovrujic, J. Biudinski-Simendic, I. Krakovsky, D. Uskokovic, Evaluation of hot-presses hydroxyapatite/poly-L-lactide composite biomaterial characteristics, J. Biomed. Mater. Res. B Appl. Biomater. 71 (2004) 284–294, https://doi.org/10.1002/jbm.b.30093.

[32] M. Cristea, D. Ionita, M.M. Iftime, Dynamic mechanical analysis investigations of PLA-based renewable materials: how are they useful? Materials 13 (2020) 5302, https://doi.org/10.3390%2Fma13225302.

[33] K.L.M. Avegnon, A.M. Bedke, J.D. Minyard, M.R. Garda, L. Delbreilh, B. Vieille, M. Negahban, M.P. Sealy, Use of negative thermal expansion to design scaffolds for cultured meat, Mater. Des. 242 (2024) 112992, https://doi.org/10.1016/j.matdes.2024.112992.

[34] F. Hassouna, J.M. Raquez, F. Addiego, P. Dubois, V. Toniazzo, D. Ruch, New approach on the development of plasticized polylactide (PLA): grafting of poly (ethylene glycol)(PEG) via reactive extrusion, Eur. Polym. J. 47 (2011) 2134–2144, https://doi.org/10.1016/j.eurpolymj.2011.08.001.

[35] D. Li, Y. Jiang, S. Lv, X. Liu, J. Gu, Q. Chen, Y. Zhang, Preparation of plasticized poly (lactic acid) and its influence on the properties of composite materials, PLoS One 13 (2018) e0193520, https://doi.org/10.1371/journal.pone.0193520.

[36] R.M. German, Chapter One – Introduction. Sintering: from Empirical Observations to Scientific Principles, Butterworth-Heinemann, 2014, pp. 1–12, https://doi.org/10.1016/B978-0-12-401682-8.00001-X.

[37] R.A. Maier, In situ observation of the multistep process of cold sintering, J. Am. Ceram. Soc. 107 (2024) 6544–6553, https://doi.org/10.1111/jace.19947.

[38] M. Puchalski, S. Kwolek, G. Szparaga, M. Chrzanowski, I. Krucińska, Investigation of the influence of PLA molecular structure on the crystalline forms (α’and α) and mechanical properties of wet spinning fibres, Polymers 9 (2017) 18. ⟨https://www.mdpi.com/2073-4360/9/1/18#⟩.

[39] T. Tábi, S. Hajba, J.G. Kovács, Effect of crystalline forms (α′ and α) of poly (lactic acid) on its mechanical, thermo-mechanical, heat deflection temperature and creep properties, Eur. Polym. J. 82 (2016) 232–243, https://doi.org/10.1016/j.eurpolymj.2016.07.024.

[40] S. Zhou, X. Zheng, X. Yu, J. Wang, J. Weng, X. Li, B. Feng, M. Yin, Hydrogen bonding interaction of poly (D, L-lactide)/hydroxyapatite nanocomposites, Chem. Mat. 19 (2007) 247–253, https://doi.org/10.1021/cm0619398.

[41] H.W. Lee, R. Insyani, D. Prasetyo, H. Prajitno, J. Sitompul, Molecular weight and structural properties of biodegradable PLA synthesized with different catalysts by direct melt polycondensation, J. Eng. Technol. Sci. 47 (2015) 364–373, https://dx.doi.org/10.5614%2Fj.eng.technol.sci.2015.47.4.2.

[42] J. Muller, A. Jiménez, C. González-Martínez, A. Chiralt, Influence of plasticizers on thermal properties and crystallization behaviour of poly (lactic acid) films obtained by compression moulding, Polym. Int. 65 (2016) 970–978, https://doi.org/10.1002/pi.5142.

[43] J.Y. Rho, T.Y. Tsui, G.M. Pharr, Elastic properties of human cortical and trabecular lamellar bone measured by nanoindentation, Biomater 18 (1997) 1325–1330, https://doi.org/10.1016/S0142-9612(97)00073-2.

[44] M. Semaan, E. Karam, C. Baron, M. Pithioux, Estimation of the elastic modulus of child cortical bone specimens via microindentation, Connect. Tissue Res. 60 (2019) 399–405, https://doi.org/10.1080/03008207.2019.1570170.